5-3. Contract Beamlines

BL22XU
(JAEA Actinide Science I)

1. Introduction

BL22XU was constructed as JAEA's fourth beamline (the hard X-ray undulator beamline) in the Storage Ring and the RI Laboratory to research radioactive materials containing transuranium elements. BL23SU and BL22XU are complementary. BL22XU promotes basic and applied research on nuclear energy and Fukushima environmental recovery research.

Because the original monochromator had difficulty measuring spectra, especially XAFS measurements, the monochromator was replaced during the summer maintenance period in FY2018. The new one is a cam-type monochromator with a multi-crystal switching system [1-2]. Si(111) and Si(311) crystals can be arbitrarily switched in a vacuum and in a low-temperature environment. This monochromator is applicable for X-rays of 6–70 keV. The start-up operations of the monochromator are complete and it has been operational since late November 2018.

In addition, the experimental equipment to promote Fukushima environmental recovery research and 1F decommissioning research will be relocated and optimized for BL22XU.

2. Experimental hutch 1

2-1. High-pressure high-temperature apparatus for monochromatic X-ray experiments

A cubic-type multi-anvil press apparatus can generate pressures up to 10 GPa and temperatures up to 2000 K. With this press, angle-dispersive X-ray diffraction (ADX) measurements and density measurements using X-ray absorption are possible. To expand the pressure region of the density measurement, the Osaka University group applied this measurement technique using the multi-anvil press to measurements using a diamond anvil cell [3]. With an external heating system, the density of liquid Ga metal could be obtained up to 10 GPa and 500 K. Density measurements over a wide range of high temperature and high pressure indicate that the equation of state of high temperature can be obtained accurately even for liquid and amorphous materials.

2-2. Diamond anvil cell diffractometer

The diamond anvil cell diffractometer is designed for both single crystal and powder X-ray diffraction experiments under high pressure and low temperature. To obtain pair-distribution function (PDF) data, X-ray total scattering measurements up to Q = 27 Å^{-1} were recently performed using high-energy monochromatic X-rays and a large-size two-dimensional detector in ambient and hydrogen gas environments. Because PDF is a powerful tool to investigate local to middle range structures, both the number of users for X-ray total scattering measurements and their targets have increased [4-8].

We improved the sample stage. It can now change sample capillary cells quickly. To improve the quality of the obtained total scattering as well as

PDF data, the PIXIA and MaterialsPDF program [9] developed by Dr. Tominaka were installed. Then we optimized the parameters of the PIXIA program for this diffractometer.

3. Experimental hutch 3

3-1. Hard X-ray photoelectron spectroscopy (HAXPES)

(1) Decommissioning research of Fukushima Daiichi Nuclear Power Plant

Chemical reactions between fission products (FPs) and structural materials in nuclear reactors are key factors to understand the FP transport behaviors during a severe accident (SA) and to improve source term analysis codes [10]. Knowledge about the detailed chemical properties of FPs on the surface of structural materials of a reactor is also useful for the decommissioning of the Fukushima Daiichi Nuclear Power Plant. Among various FPs, cesium (Cs) is especially important due to its high radiological impacts, high radiation dose, and high chemical reactivity [11]. Since the major structural material in the reactor is stainless steel (SS), information about the adsorption behavior of Cs on SS and the identification of the chemical forms of Cs products in the surface layers are crucial.

We measured HAXPES spectra on the cross-section samples of Cs-adsorbed SS substrates prepared at 800 degrees under a H_2O/Ar-5%H_2 atmosphere (simulated SA condition) to observe the electronic states of the constituent elements such as Cs and to identify the chemical form of the reaction products. By focusing an incident X-ray beam within 2–3-μm diameter, the spatial variations in the electronic states with depth of the cross section are observed. That is, the spatial distribution of the reaction products is determined as a function of depth.

We also investigated the difference of the Cs adsorption behavior for two contents of the SS substrate: 0.2 wt% and 4.9 wt%. In this study, to understand the Cs adsorption behavior on structure materials in SA in a light-water nuclear reactor, the chemical state of Cs and its distribution on the surface of SS with different Si concentrations were investigated by HAXPES. Cs is selectively adsorbed at the site where Si is distributed with a high concentration. $CsFeSiO_4$ is the dominant Cs products in case of a low Si content, while $CsFeSiO_4$, $Cs_2Si_2O_5$, and $Cs_2Si_4O_9$ are formed in the case of a high Si content. The chemical forms of the Cs compounds produced in the adsorption process on the SS surface are closely correlated with the concentration and chemical states of Si originally included in SS [12].

(2) Electronic structures of Pt/$Y_3Fe_5O_{12}$ (YIG) bilayers

We used prototypical devices utilizing the spin Seebeck effect (SSE), which refers to the generation of a spin current arising from a temperature gradient in a magnetic material [13]. One of the most extensively studied systems, Pt/$Y_3Fe_5O_{12}$ (YIG) junction, exhibits unconventional electronic transport phenomena such as an unconventional Hall effect [14]. A possible origin is the presence of Fe impurities from YIG either in the Pt layer or at the Pt/YIG interface, which behave as independent paramagnetic moments [14].

To elucidate the mechanism of this behavior, the HAXPES spectra were measured [15]. Figure 1 shows the spectra in the Fe 1*s* region for both YIG and the samples with thin Pt layers of 2 nm and 5 nm. The Pt/YIG samples have two components at a

binding energy (BE) of 7,115–7,110 eV. The large peak with BE ~ 7,114 eV is assigned to Fe^{3+} based on the data of YIG, in which the peak at 7,122 eV may be rooted in the energy loss. On the other hand, the other small peak at a lower BE of ~7,112 eV is due

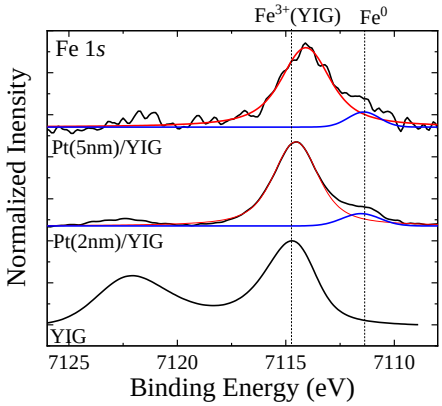

Fig. 1. Fe 1*s* HAXPES spectra for the samples with the two thin Pt layers as well as YIG. Two dotted lines represent the binding energies of Fe^{3+} and Fe^{0} states. Red and blue solid lines stand for the components for Fe^{3+} and Fe^{0}, respectively, which are obtained from the peak deconvolution.

to metallic Fe (Fe^{0}). This result supports the proposed origin of the anomalous Hall effect. That is, metallic Fe can act as a paramagnetic impurity in the Pt layer, giving rise to a skew scattering or itinerant electrons in Pt [14, 15].

3-2. Stress / imaging measurements

In this device, deformation and state changes inside a material are performed by a diffraction method and an imaging method using high-energy synchrotron radiation X-rays. Figure 2 shows the captured longitudinal behavior of an aluminum alloy A1050 weld pool during the pool formation process [16]. Laser welding is an efficient way to achieve high-quality products. Here, the quality of the product is determined by the interaction between the laser and the material. However, this interaction cannot be observed directly because keyholes and molten metal induced by high-power density lasers are surrounded by solid metal. Therefore, *in situ* observations of internal phenomena were performed using a high-energy synchrotron radiation imaging method. In 1 ms, a keyhole with

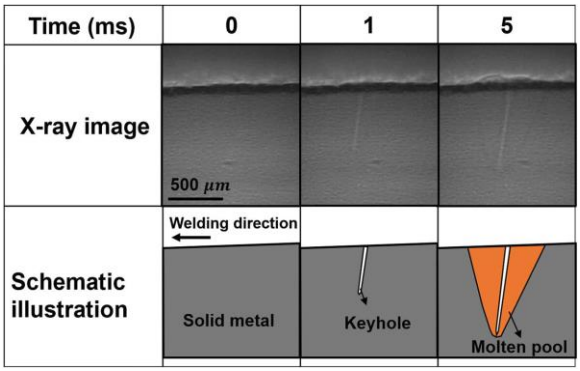

Fig. 2. Dynamic longitudinal view of a weld pool during the pool formation process captured by the X-ray imaging system (A1050).

a large depth-to-diameter ratio was produced, but the weld pool surrounding the keyhole was unclear, indicating that the growth rate of the keyhole is higher than the growth rate of the molten pool at this point. At 5 ms, a large area of the molten pool appears around the keyhole. During this process, heat is transferred from the metal on the keyhole wall to the metal surrounding the keyhole, gradually forming a molten metal surrounding the keyhole. The trapped behavior of the weld pool demonstrates that the heat of the laser is first absorbed into the keyhole and then transferred to the metal surrounding the keyhole.

3-3. ASAXS

An experimental system for anomalous small-angle X-ray scattering (ASAXS) was developed in experimental hutch 3. ASAXS measurements of steels were performed to characterize the elemental dispersion of Cr, which is crucial to understand corrosion resistance and embrittlement in steels.

3-4. Large diffractometer

An apparatus for Bragg coherent X-ray diffraction imaging (Bragg-CDI) was constructed. To evaluate its performance, we prepared two types of sample particles: one with cubic-like shapes and the other with particles rich in curved surfaces. The shapes and sizes of the particles were successfully reconstructed, and are consistent with the results from the scanning electron microscope (SEM) measurements previously performed. Furthermore, details of the internal structure such as the strain and reverse surface of the particles were obtained. This information was not available from SEM measurements. Our technique can be used to study particles as small as 100 nm [17]. Bragg-CDI should be a powerful technique to investigate an individual nanosized crystalline particle and will open the door for studies on a particle located within devices, which is inaccessible by electron beam techniques.

Hideaki Shiwaku[*1], Akihiko Machida[*2], Tetsu Watanuki[*2], Masaaki Kobata[*1], Kenji Yoshii[*1], Tetsuo Okane[*1], Takahisa Shobu[*1], Yojiro Oba[*1], Kenji Ohwada[*2]

[*1] Japan Atomic Energy Agency

[*2] National Institutes for Quantum and Radiological Science and Technology

References:

[1] H. Shiwaku et al., *AIP Conference Proceedings* **705**, 659 (2004)

[2] H. Shiwaku et al., *JAEA-Research*-2009-009

[3] Y. Takubo et al., *High Press. Res.* **38**, 406-413 (2018).

[4] K. Sakaki et al., *J. Alloys Compds.* **750**, 33-41 (2018).

[5] T. Nishikubo et al., *Appl. Phys. Express* **11**, 061102 (2018).

[6] K. Sakaki et al., *J. Appl. Cryst.* **51**, 796-801 (2018).

[7] Y. Ide et al., *Chem. Sci.* **9**, 8637-8643 (2018).

[8] K. Asano et al., *Inorg. Chem.* **57**, 11831-11838 (2018).

[9] S. Tominaka et al., *ACS Omega* **3**, 8874 (2018).

[10] F. Martin-Fuertes et al., *Nucl. Eng. Des.* **237** (5), 509-523 (2007).

[11] S. Miwa et al., *Energy Procedia* **71**, 168-181 (2015).

[12] M. Kobata et al., *J. Nucl. Mate.* **498**, 387-394 (2018).

[13] K. Uchida et al., *Nature Mater.* **9**, 894-897 (2010).

[14] T. Kikkawa et al., *Phys. Rev. B* **95**, 214416 (2017).

[15] M. Kobata et al., *JPS Conf. Proc.*, **30**, 011192 (2020).

[16] M. Miyagi et al., *Scientific Reports* **8**, 12944 (2018).

[17] K. Ohwada et al., *Jpn. J. Appl. Phys.* **58**, SLLA05 (2019).